Accepted Manuscript

Electronic structure of bulk AnO$_2$ (An = U, Np, Pu) and water adsorption on the (111) and (110) surfaces of UO$_2$ and PuO$_2$ from hybrid density functional theory within the periodic electrostatic embedded cluster method

Joseph P.W. Wellington, Andrew Kerridge, Jonathan Austin, Nikolas Kaltsoyannis

Please cite this article as: J.P.W. Wellington, A. Kerridge, J. Austin, N. Kaltsoyannis, Electronic structure of bulk AnO$_2$ (An = U, Np, Pu) and water adsorption on the (111) and (110) surfaces of UO$_2$ and PuO$_2$ from hybrid density functional theory within the periodic electrostatic embedded cluster method, *Journal of Nuclear Materials* (2016), doi: 10.1016/j.jnucmat.2016.10.005.
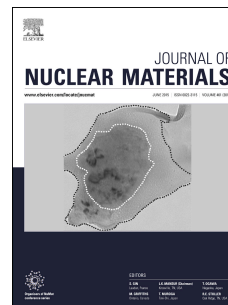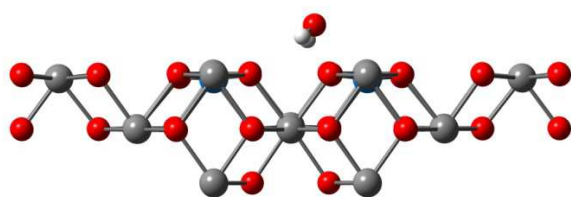
The electronic structures of AnO_2 (An = U, Np, Pu) are studied computationally with hybrid density functional theory, and the geometries and energetics of water adsorption on the low index surfaces are presented.

Electronic structure of bulk AnO$_2$ (An = U, Np, Pu) and water adsorption on the (111) and (110) surfaces of UO$_2$ and PuO$_2$ from hybrid density functional theory within the periodic electrostatic embedded cluster method

Joseph P. W. Wellington[1], Andrew Kerridge[2], Jonathan Austin[3] and Nikolas Kaltsoyannis*[4]

[1]Department of Chemistry, University College London,

20 Gordon Street, London WC1H 0AJ, UK

[2]Department of Chemistry, Lancaster University,

Bailrigg, Lancaster LA1 4YP, UK

[3]National Nuclear Laboratory, Chadwick House, Warrington Road, Birchwood Park,

Warrington, WA3 6AE

[4]School of Chemistry, The University of Manchester,

Oxford Road, Manchester, M13 9PL, UK

*nikolas.kaltsoyannis@manchester.ac.uk

1

Abstract

Generalised gradient approximation (PBE) and hybrid (PBE0) density functional theory (DFT) within the periodic electrostatic embedded cluster method have been used to study AnO_2 bulk and surfaces (An = U, Np, Pu). The electronic structure has been investigated by examining the projected density of states (PDOS). While PBE incorrectly predicts these systems to be metallic, PBE0 finds them to be insulators, with the composition of the valence and conduction levels agreeing well with experiment. Molecular and dissociative water adsorption on the (111) and (110) surfaces of UO_2 and PuO_2 has been investigated, with that on the (110) surface being stronger than on the (111). Similar energies are found for molecular and dissociative adsorption on the (111) surfaces, while on the (110) there is a clear preference for dissociative adsorption. Adsorption energies and geometries on the (111) surface of UO_2 are in good agreement with recent periodic DFT studies using the GGA+U approach, and our data for dissociative adsorption on the (110) surface of PuO_2 match experiment rather well, especially when dispersion corrections are included.

Introduction

The electronic structure of the actinide oxides is complicated, as these systems can exhibit either electron localization or delocalization as well as having partially occupied f levels. For the actinide dioxides the 5f levels move to lower energies as the actinide series is crossed; for ThO_2, which has no 5f electrons, the unoccupied 5f levels are located in the 6d conduction band. For UO_2 the occupied 5f levels are in the gap between the occupied oxygen 2p levels and the unoccupied U 6d levels, and these 5f levels are seen from photoelectron spectroscopy (PES) to comprise the valence band[1]. In addition the unoccupied 5f levels are now lower in energy than the U 6d levels, and they form the conduction band, as shown by X-ray adsorption spectroscopy (XAS)[2]; thus UO_2 is a Mott-Hubbard insulator with f-f transitions. When PuO_2 is reached the occupied 5f levels have lowered further in energy and are now located at the top of the occupied oxygen 2p band, as seen from PES[3]. PuO_2 is also an insulator; however, as the top of the valence band now has oxygen character it is no longer a Mott-Hubbard insulator but a ligand to metal charge transfer (LMCT) insulator.

The 3d, 4f and 5f electrons in first row transition metal, lanthanide and actinide oxides, respectively, are strongly correlated and therefore are localized on the metals ions. Density functional theory (DFT) within the local density approximation (LDA) or generalised gradient approximation (GGA) describes these systems poorly; in the case of the actinide dioxides such approaches predict metallic behaviour[4,5]. Alternative methods within DFT have been employed in order to obtain the insulating character of these systems, including DFT+U[2,6–8], self-interaction corrections

(SICs)[9], DFT+ dynamical mean field theory (DMFT)[10,11] and hybrid functionals.[5,12]

AnO_2 (An = U, Np, Pu) adopt the fluorite (CaF_2) structure, in which the actinide ions are 8 coordinate, whilst oxygen ions lie in a tetrahedral 4 coordinate environment. The (111) oxygen-terminated surface is the most stable surface of fluorite AnO_2; the surface actinide ions are 7- and the oxygen ions 3-coordinate. The (110) surface is the second most stable of the AnO_2 surfaces; it is formed of stoichiometric layers in which the surface actinide ions are 6- and the oxygen ions 3-coordinate. Atomistic studies have shown that although the clean (111) surface is the most stable UO_2 surface, hydroxylation lowers the energies of the (110) and (100) faces, so that at high coverage the hydroxylated (100) surface is the most stable[13,14]. These results have also been found from a DFT+U study where the stability of the three low index, fully hydroxylated surfaces was reversed compared with the clean surfaces, with (100) > (110) > (111)[15].

Water is known to adsorb weakly and reversibly on UO_2 (111) single crystal surfaces[16] and thin films.[17] If the UO_2 surface is sputtered (creating a substoichiometric UO_{2-x} surface) prior to water adsorption, then H_2 desorbs from the surface.[16] Similarly, temperature programmed desorption (TPD) experiments with D_2O reveal that D_2 also desorbs from polycrystalline UO_2 surfaces.[18] Hence on substoichiometric or polycrystalline UO_2—where many defects are present—dissociative adsorption of water occurs followed by H_2/D_2 desorption.

Of the world's c. 250 tonnes of separated civil plutonium, more than 100 tonnes are stored at Sellafield in the UK as PuO_2 powder in sealed steel cans. Under certain

circumstances, gas generation may occur in these cans, with consequent pressurization. This is one of the most serious fault scenarios to be considered in the safety cases for PuO_2 storage. Several routes to gas production have been suggested, including (i) steam produced by H_2O desorption from hygroscopic PuO_2 (ii) radiolysis of adsorbed water (iii) generation of H_2 by chemical reaction of PuO_2 with H_2O, producing a PuO_{2+x} phase and (iv) generation of He gas resulting from alpha decays within the PuO_2. In addition, the PuO_2 surface can act as a catalyst towards the recombination of gases to their more stable chemical form. Many of these processes involve PuO_2/H_2O interactions, and are complex, inter-connected and poorly understood.

Experimental studies of water adsorption on PuO_2, obtained from various means including interim storage, have shown that water adsorbs *via* a multi-step process with initial strong chemisorption due to dissociation, forming a hydroxylated surface, followed by successive layers of H_2O physisorbed above the hydroxylated layer[19]. Stakebake found, from a TPD study on PuO_2 prepared from Pu metal, that water desorbed in two temperature ranges, one between 373–423 K, and a second between 573–623 K.[20] It was assumed that the reversible adsorption of water is a non-activated process and so the enthalpy of adsorption is equal to the activation energy of desorption. He attributed the higher temperature desorption to dissociatively adsorbed water forming a hydroxylated layer, estimating an adsorption energy of -2.94 eV, whilst the lower temperature was thought to be due to molecular water hydrogen bonded to the hydroxyl layer, with an estimated adsorption energy of -0.88 eV. Paffet *et al.* revised these estimations based on a Redhead analysis of the results, estimating adsorption energy values of -1.82 eV for dissociative adsorption and -1.11 eV for water molecularly adsorbing to the hydroxyl layer at 371 K.[21]

5

Theoretical studies have disagreed as to whether molecular or dissociative adsorption is more energetically favourable on the (111) surface of UO$_2$. Skomurski *et al.*[22] and Weck *et al.*[23] both found molecular adsorption to be more favourable, with adsorption energies of c. -0.7 (-0.25 for 1 monolayer (ML)) and -0.8 eV, whilst dissociative adsorption energies were lower with -0.4 (-0.22 for 1 ML) and -0.6 eV for a coverage of ½ ML. More recent studies have found dissociative adsorption to be more favourable at low coverage of ¼ ML, by 0.02 eV[24] and 0.07 eV[25], with an adsorption energy of -1.12 eV[24] and -0.68 eV[25] for dissociative adsorption. However, at higher coverage a mixture of molecular and dissociative adsorption was found to be the most favourable arrangement. Other studies have focused on the hydroxylated surface, calculating dissociative adsorption energies of -0.29 eV[15] and -1.08 eV[26] for 1 ML coverage.

Adsorption on the (110) surface of UO$_2$ is less well studied, but dissociative adsorption energies of -1.05 eV[15] and -0.93 eV[25] were obtained from DFT+*U* studies of 1 ML coverage, with the adsorption 0.76 eV[15] and 0.61 eV[25] stronger than on the (111) surface—as expected due to the higher surface energy of the (110) surface. The more recent study by Bo *et al.* calculated mixtures of molecular and dissociative adsorptions.[25] Whilst they found the fully hydroxylated surface to be more stable than molecular water covering the surface, they concluded that a mixture of the two was the most favourable at a surface coverage of 1 ML.

In addition to the UO$_2$ work, there are periodic boundary conditions (PBC) DFT studies on PuO$_2$, either comparing water adsorption on different actinide dioxides[15,26] or looking solely at the PuO$_2$ surfaces[27,28]. The two studies comparing water adsorption on different actinide oxide surfaces both examine

6

dissociative adsorption forming a fully hydroxylated surface. Both find dissociative adsorption to be more favourable on UO_2 than PuO_2, by 0.22 eV[26] or 0.06 eV[15] on the (111) surface and 0.08 eV[15] on the (110) surface. Additionally, dissociative water adsorption was seen to be more favourable by 0.74 eV on the (110) than the (111) surface[15]. The other two theoretical studies focusing solely on PuO_2 considered only the (110) surface. Both found dissociative adsorption to be more favourable than molecular, by 0.11 eV[28] and 0.16 eV[27] for a full layer of coverage. The dissociative adsorption energies range from -0.23 to -0.86 eV on the (111) surface and from -0.01 to -0.95 eV on the (110) surface.

The theoretical studies described above focus primarily on PBC calculations. In this approach a unit cell representing a portion of the surface is repeated infinitely in two dimensions; however to study a coverage of water lower than 1 monolayer (ML), or water not adsorbing uniformly, large unit cells must be used. This can significantly increase the computational time required, particularly if hybrid functionals are needed to describe the system. In this study we employ the periodic electrostatic embedded cluster method (PEECM),[29] in which a portion of the surface is described quantum mechanically and the rest of the system is approximated by point charges. Our study is the first use of the PEECM to study AnO_2. Although the PEECM has certain limitations, *i.e.* it does not allow the optimization of lattice parameters, the positions of atoms at the edge of the quantum mechanically treated cluster must be held fixed, and care must be taken to limit polarization effects at the cluster boundary, it offers certain advantages over PBC approaches. In particular it is relatively straightforward to employ hybrid DFT, thus avoiding the need for a Hubbard *U* correction factor. We examine the electronic structure of bulk AnO_2 as well as the adsorption of water on the (111) and (110) surfaces of UO_2 and PuO_2.

7

We have previously used the PEECM when investigating environmental effects on the electron density topology of $Cs_2UO_2Cl_4$, $U(Se_2PPh_2)_4$ and $Np(Se_2PPh_2)_4$ and have very recently reported a limited preliminary dataset from the present study as a contribution to the 2016 Waste Management Conference[30] (absorption of a single water molecule on a cluster representation of the UO_2 (111) surface).

Computational details and methodology

All calculations were performed with the TURBOMOLE 6.5 program[31]. The PBE[32] (GGA) and PBE0[33] (hybrid-GGA) exchange-correlation functionals were used for single-point calculations of bulk actinide oxide systems; as we show, PBE0 performs well here and hence it was used for all surface calculations.

The self-consistent field convergence was set to 1×10^{-6} a.u. whilst geometry optimizations were performed with convergence criteria of 1×10^{-6} a.u. for the total energy and 1×10^{-3} a.u. for the maximum norm of the cartesian energy gradient.

For cluster calculations simulating bulk AnO_2 the def-SV(P) basis sets[34,35] contained in the TURBOMOLE library were used for all oxygen atoms and actinides that used a small core pseudopotential (PP) (see below), and the double-zeta MWB-AVDZ[36] basis set was used for actinide atoms using a large core PP. For water adsorption calculations the def-SV(P) and MWB-AVDZ basis sets were again used, with the corresponding small and large core PPs, noted from now on as the SV(P) basis set. Single point calculations were performed, at geometries obtained with the SV(P) basis set, with the larger def-QZVP[35,37] and MWB-AVQZ[36] basis sets,

used with the corresponding small and large core PPs, noted now as the QZVP basis set.

PPs were used for the actinide ions in the quantum mechanically treated cluster; small-core (60 electron) def-PPs from the TURBOMOLE library[38,39] or, where stated, large-core PPs incorporating the 5f electrons,[36] corresponding to 80, 81 or 82 electron cores for U, Np and Pu respectively—these are electrons with principal quantum number 5 or lower. These 5f-in-core PPs have been parameterized specifically for tetravalent states. When the 5f-in-core PPs are used the clusters are written as $An_xAn_yO_{2(x+y)}$ where x refers to the number of actinide ions with explicit 5f electrons and y to the number of actinide ions described by 5f-in-core PPs.

Density of states (DOS) diagrams were produced for the bulk AnO_2 electronic structure calculations by Gaussian smearing of Kohn-Sham orbital energies; the Fermi energy is taken as the top of the highest occupied level. The projected (P)DOS were produced by Mulliken partitioning of orbitals into s, p, d and f contributions within the TURBOMOLE 6.5 program.

Dispersion corrections have been included with the Grimme D3 parameters.[40]

All calculations were performed using the PEECM.[29] In this approach, the system is split into three regions: an inner explicit cluster region, which is treated quantum mechanically as described above; the outer embedding region, consisting of point charges; and an intermediate region, consisting of negative point charges and PPs (Figure 1). The infinite outer embedding region recreates the Madelung potential of the bulk system; formal charges were used for the ions in this region, +4 for actinide ions and -2 for oxygen ions. The PPs used in the intermediate region were the Ce

9

CRENBL PPs,[41] employed in order to avoid overpolarization of the electron density in the explicit cluster, whilst -2 charges again represent the oxygen ions. The Ce CRENBL PP, which corresponds to a +4 charge when used without any basis functions, was used since no actinide PPs corresponding to a +4 charge are available. The 8-coordinate Ce(IV) ionic radius, 0.97 Å, is very similar to that of U(IV), 1.00 Å, Np(IV), 0.98 Å and Pu(IV) 0.96 Å.[42]
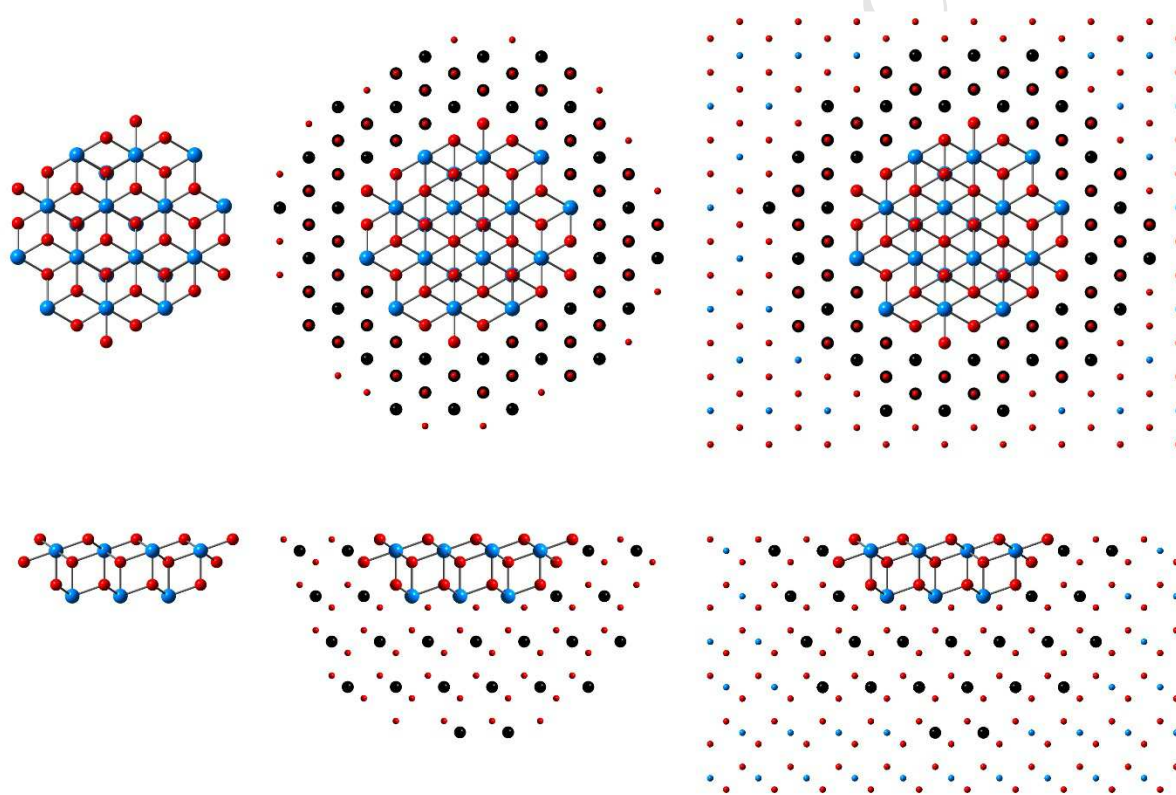

Figure 1

Representative illustration of the PEECM. The quantum mechanical cluster (left) embedded in the intermediate (middle) and outer (right) regions, viewed from above (top row) and from the side (bottom row). Large blue spheres represent explicit actinide ions, large red explicit oxygen, large black, PPs of the intermediate region, small blue actinide point charges, and small red oxygen point charges. Outer region truncated.

As lattice parameters cannot be optimized within the PEECM, experimental lattice parameters were used, a = 5.470, 5.420, 5.398 Å for UO_2, NpO_2 and PuO_2

respectively, which are all in the space group Fm $\overline{3}$ m. Theoretical values of the lattice parameter of UO_2 span a wide range of almost 0.3 Å, from 5.28 Å calculated with LDA[5], to 5.568 Å at the PBE+U level.[43] GGA+U generally overestimates AnO_2 lattice parameters *vs* experiment,[8,25,44,45], while hybrid functionals tend to slightly underestimate them.[5,46,47]. We have therefore chosen to employ the experimental values, noting that these lie within the range spanned by previous hybrid and GGA+U studies.

Within our model, the metals ions are coupled ferromagnetically, with 2, 3 or 4 unpaired electrons per actinide ion for UO_2, NpO_2 and PuO_2 respectively. *I.e.* we converge on the high spin ground state within the spin-unrestricted Kohn-Sham formalism – by no means straightforward for systems with so many unpaired 5f electrons. Bulk AnO_2 are known to be antiferromagnetically coupled, but the local magnetic ordering in a small molecular cluster of c. 20 AnO_2 units is not necessarily so, and the difference in energy between ferromagnetic and antiferromagnetic ordering in actinide oxides has been seen in previous theoretical studies to be very small, in the order of tens of meV with a hybrid functional.[7,46,47]

For the bulk electronic structure calculations, geometries were fixed at the experimental lattice structure. For surface calculations the coordinates of ions in the cluster coordinated only to other quantum mechanical ions were optimized. When performing adsorption calculations, the coordinates of the water molecules were additionally allowed to relax. Adsorption energies were calculated using the following equation, with each species being optimized as described above:

$$E_{ads} = E_{surface+H2O\ (optimized)} - E_{surface(optimized)} - E_{H2O(optimized)} \qquad (1)$$

Results and discussion

Electronic structure of AnO_2 (An = U, Np, Pu)

We began by studying the electronic structure of bulk AnO_2; single point calculations were performed on $An_{16}O_{32}$ clusters, shown in Figure 2, embedded in 3D arrays of point charges to simulate the bulk. When the PBE functional is used it can be seen from the PDOS (Figure 3) that UO_2 is predicted to be metallic, with the Fermi level cutting through the U 5f band. Hence this functional incorrectly describes the electronic structure of the system, which is experimentally characterised as a Mott-Hubbard insulator.[2]
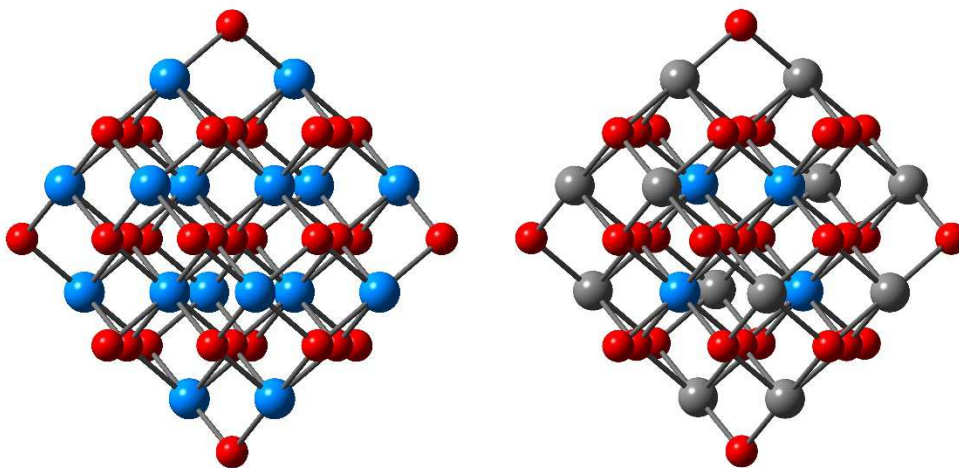

Figure 2

$An_{16}O_{32}$ cluster (left) and $An_4An_{12}O_{32}$ cluster (right), oxygen ions shown in red, actinide ions in blue and grey. Grey spheres represent actinide ions treated with 5f-in-core PPs. Embedding ions not shown.
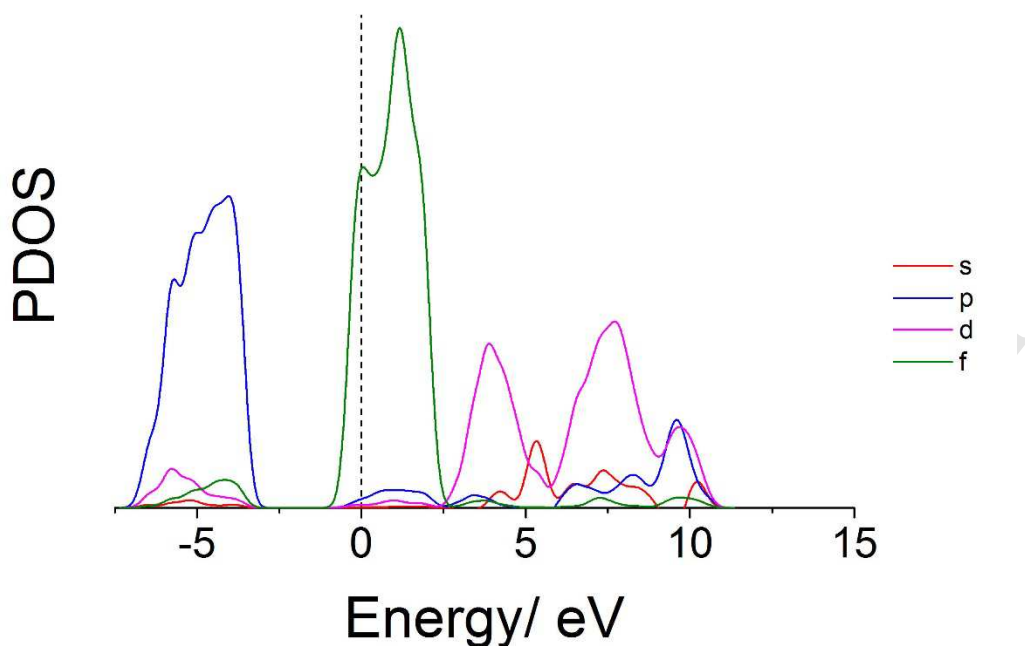
Figure 3

PDOS of bulk UO_2 modelled as a $U_{16}O_{32}$ cluster with the PEECM and the PBE functional. Vertical line shows the Fermi level. Vertical scale in arbitrary units.

When the PBE0 functional is used it can be seen from the PDOS plots, Figure 4, that each AnO_2 cluster is predicted to be an insulator. From the decomposition of the states into their s, p, d and f contributions it can be seen that UO_2 and NpO_2 have both valence and conduction levels of f character. They are hence both predicted to be Mott-Hubbard insulators, exhibiting f-f transitions. The occupied f levels in NpO_2 are more stabilized than in UO_2, lying closer in energy to the valence oxygen p levels. The HOMO-LUMO gaps are 3.2 eV and 3.6 eV for UO_2 and NpO_2 respectively, higher than the experimental band gaps of 2.1 eV[48] and 2.85 eV.[49] This overestimation arises as HOMO-LUMO gaps are between discrete energy levels and hence are not directly comparable with bulk band gaps.

PuO_2 has 5f levels that are more stable than those of UO_2 and NpO_2, with energies comparable with the highest O 2p valence levels. Thus, as noted in the introduction, PuO_2 is not a Mott-Hubbard insulator, as there is a significant contribution of oxygen

13

2p valence levels at the valence band edge. PuO$_2$ is better described as an LMCT system, in agreement with experiment.[3] The HOMO-LUMO gap for the cluster is 3.3 eV, again slightly larger than the experimental value of 2.80 eV.[49]

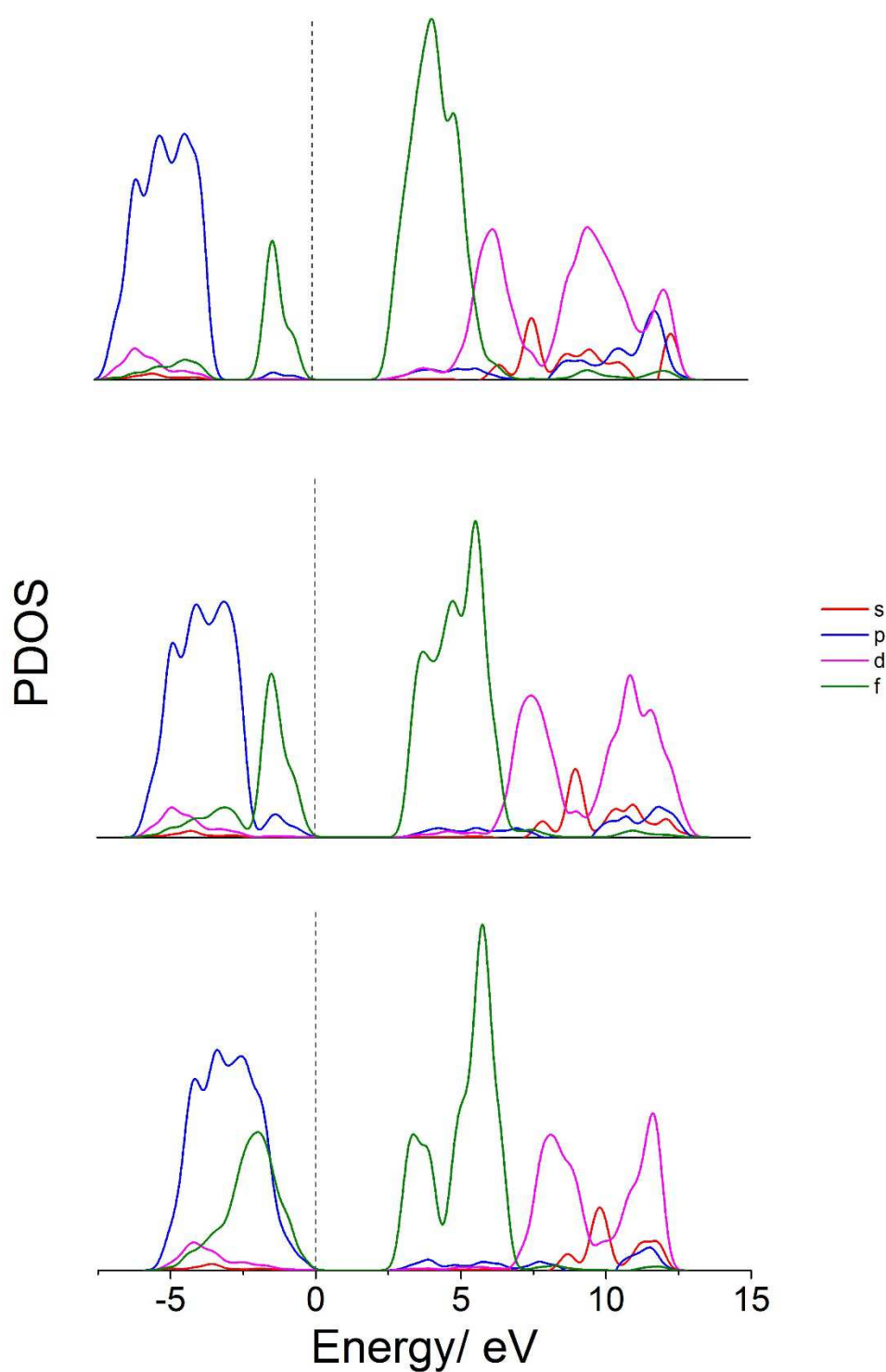**Figure 4**

PDOS of bulk AnO_2 (An = U (top), Np, Pu (bottom)) modelled as $An_{16}O_{32}$ clusters with the PEECM and the PBE0 functional. Vertical line shows the Fermi level. Vertical scale in arbitrary units.

In order to explore approaches to speeding up our calculations, the electronic structure of the $U_{16}O_{32}$ cluster was recalculated with the outer 12 uranium ions

15

described with 5f-in-core PPs, whilst the inner 4 ions were treated with explicit 5f electrons, *i.e.* $U_4U_{12}O_{32}$ (Figure 2). A similar electronic structure to that shown in Figure 4 is obtained, *i.e.* an insulator with valence and conduction 5f levels (Figure 5). The PDOS of the 5f levels is smaller due to fewer 5f electrons being described explicitly.
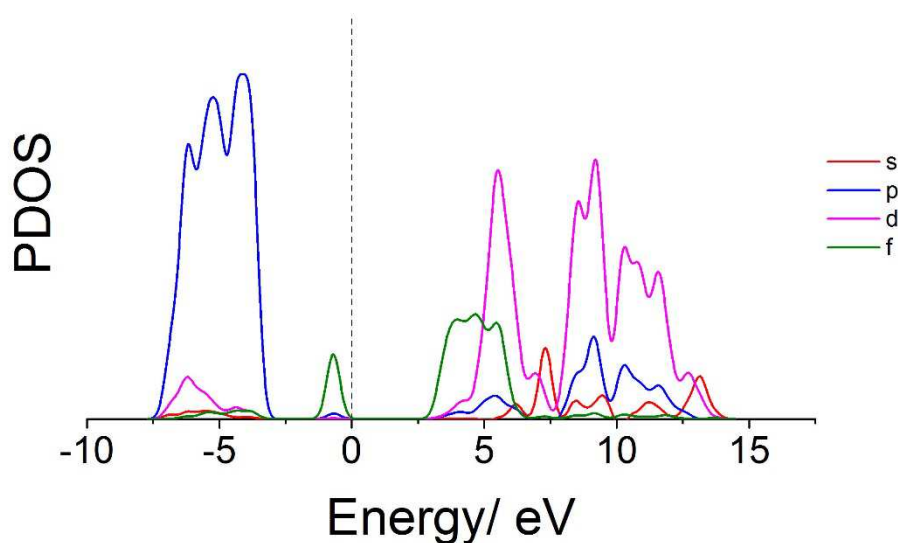
Figure 5

PDOS of bulk UO_2 modelled as a $U_4U_{12}O_{32}$ cluster (Figure 2) with the PEECM and the PBE0 functional, where 12 uranium ions are described with 5f-in-core PPs. Vertical line shows the Fermi level. Vertical scale in arbitrary units.

The spin densities were calculated and are shown for $U_{16}O_{32}$ and $U_4U_{12}O_{32}$ in Figure 6. The unpaired electrons are clearly localized on the uranium ions; in the case of the $U_4U_{12}O_{32}$ cluster the unpaired electrons are localized on the four uranium ions which treat the 5f electrons explicitly. The spin densities, from Mulliken analysis, of each uranium ion in the $U_{16}O_{32}$ cluster range from 2.04-2.07, with the f contribution to this spin density being 1.99-2.00, *i.e.* two unpaired f electrons on each uranium ion. The spin densities of the four inner uranium ions of the $U_4U_{12}O_{32}$ cluster are

16

similar to that of $U_{16}O_{32}$, with the number of unpaired electrons and their 5f level contribution differing by less than 0.03.
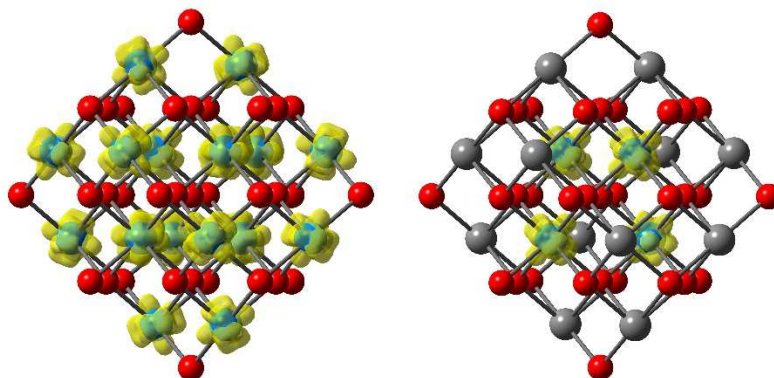

Figure 6

Spin density, shown in yellow, of $U_{16}O_{32}$ (left) and $U_4U_{12}O_{32}$ (right), oxygen ions shown in red. Grey spheres represent uranium ions treated with 5f-in-core PPs.

In summary, the insulating nature of AnO_2 is correctly calculated when using the hybrid PBE0 functional, with the composition of the valence and conduction bands agreeing with experimental and previous theoretical results. As the PBE functional incorrectly describes the electronic structure, the PBE0 functional, although more expensive, is used throughout the rest of the study. It has also been shown that when describing the cluster with a subset of actinide ions described by 5f-in-core PPs the correct electronic structure is still obtained, whilst significantly reducing the computational expense.

Water adsorption on the (111) surface of AnO_2 (An = U, Pu)

Geometries

Adsorption geometries were optimized with the SV(P) basis set. Two recent periodic DFT papers probe the adsorption of 1-4 water molecules in their supercells, which corresponds to ¼ to 1 ML of coverage on the surface.[24,25] To aid comparison with

17

the work in those papers we have investigated the adsorption of one to four water molecules on an $An_4An_{15}O_{38}$ cluster representation of the (111) surface (Figure 7) with different ratios of molecular and dissociative adsorption. This cluster contains four actinide sites which are coordinated by only the inner cluster region; these are the sites where adsorption is considered, the rest of the actinide atoms use 5f-in-core PPs.
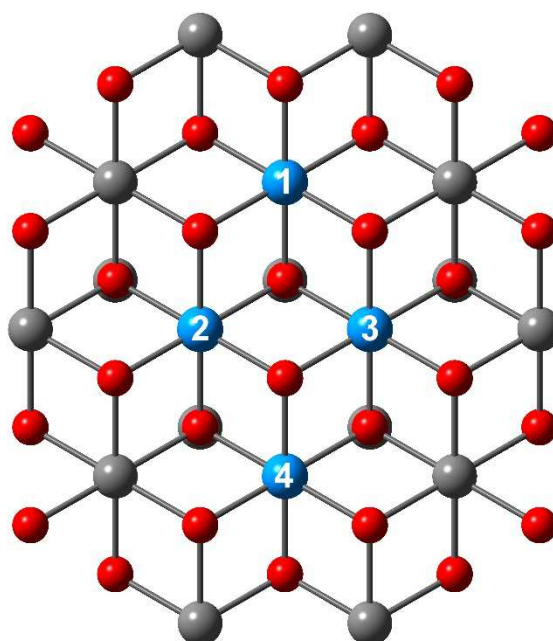
Figure 7

$An_4An_{15}O_{38}$ cluster representation of the (111) surface, viewed perpendicular to the surface. Oxygen atoms are shown in red and actinide atoms in blue and grey. Grey spheres represent actinide atoms treated with 5f-in-core PPs. Embedding ions not shown. Sites where adsorption is considered are labelled 1 to 4.

Our (111) cluster has three layers of oxygen atoms (Figure 8). The surface layer contains 14 atoms, eight of which can relax during geometry optimizations. The second layer also contains 14 atoms, of which five can relax during geometry

optimizations, and the last oxygen layer contains 10 atoms, two of which can relax during geometry optimizations. There are 14 actinide atoms in the surface layer, eight of these are allowed to relax during geometry optimizations, and there is one subsurface layer of five actinide atoms, all of which are held fixed during geometry optimizations.

Water can adsorb onto AnO_2 surfaces in two ways: molecularly, where the water molecule remains intact on adsorption, or dissociatively, where an O-H bond is heterolytically broken. Molecular adsorption on the (111) surface occurs with an oxygen adsorbing above an actinide ion and two hydrogen atoms pointing towards two surface oxygen atoms. Dissociative adsorption forms two hydroxyl groups: a hydroxide, formed from a hydrogen of the water molecule binding to a surface oxygen, which will be referred to as the surface hydroxide, and a second in which an OH group of water adsorbs above an actinide ion, which will be referred to as the adsorbed hydroxide. These adsorptions, at site 1, are shown in Figure 8. The oxygen atom in a water molecule will be referred to as O_W, oxygen in an adsorbed hydroxyl O_{OH} and oxygen at the surface O_S.
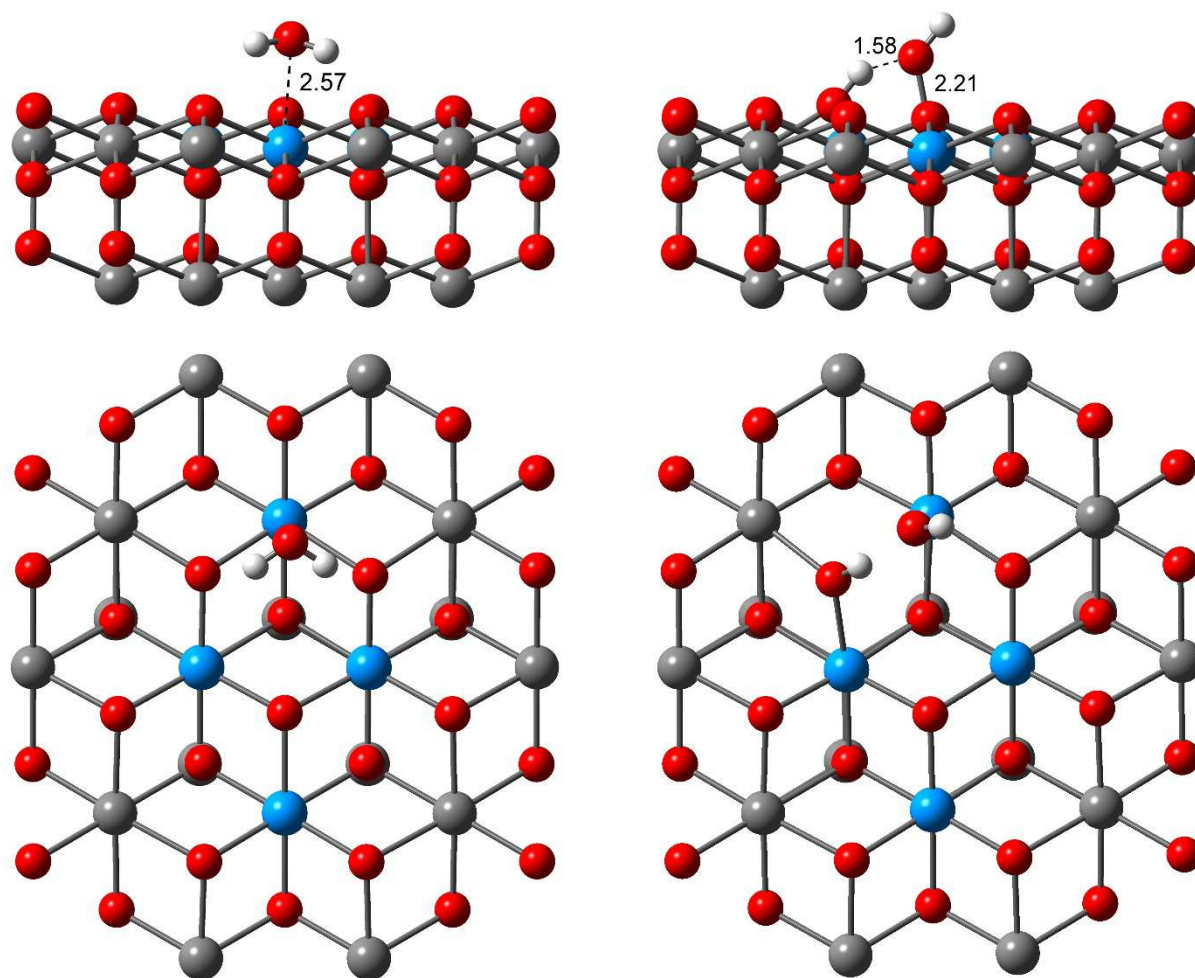
Figure 8

Molecular (left) and dissociative (right) adsorption of a single water molecule on the (111) surface of a $U_4U_{15}O_{38}$ cluster. Top view shows the cluster in the plane of the surface, whilst the bottom view is perpendicular to the surface. Hydrogen atoms are shown in white, oxygen atoms in red and uranium atoms in blue and grey. Grey spheres represent uranium atoms treated with 5f-in-core PPs. Embedding ions not shown.

In order to probe the effect of the 5f-in-core PPs on the geometries obtained, we optimized the geometries of one water molecule adsorbing either molecularly or dissociatively on the $U_{19}O_{38}$ cluster (where no 5f-in-core PPs are used). The geometries of the dissociative adsorption are affected very little; the $U-O_{OH}$ bond for dissociative adsorption differs by only 0.02 Å. For molecular adsorption, we observe a bigger variation in the two $H-O_S$ distances. The adsorption energies, however, vary

20

by no more than 0.04 eV between the 5f-in-core system and the all-explicit 5f electron analogue.

We have previously reported the geometries of single molecular and single dissociative adsorption on the UO_2 (111) surface[30], and briefly summarise the results here to facilitate comparison with the much more extensive datasets presented below. Molecular adsorption occurs with the oxygen of the water molecule above a surface uranium atom at an empty oxygen site, restoring the coordination of the surface uranium to 8. The $U-O_W$ distance for molecular adsorption is 2.57 Å, lying between recently calculated distances of 2.48 Å[24] and 2.60 Å,[25] whilst the $H-O_S$ distance is 1.76 Å, slightly longer than previously calculated values of 1.72 Å[24] and 1.61 Å.[25] This short $H-O_S$ distance shows that a hydrogen bond is formed between a hydrogen of the water molecule and an oxygen surface atom. The second $H-O_S$ distance is longer at 1.99 Å.

For dissociative adsorption the hydrogen of the surface hydroxyl points towards the oxygen of the adsorbed hydroxyl (Figure 8), with a distance of 1.58 Å; hence there is a hydrogen bond between the two OH species. Recent theoretical studies calculated H-OH distances of 1.45 Å[24] and 1.66 Å[25] on the UO_2 surface. The $U-O_{OH}$ distance is 2.21 Å and agrees very well with recent theoretical studies which found distances of 2.23 Å[24,25] and 2.24 Å[15]. The $U-O_{OH}$ is relatively short, 0.16 Å shorter than the experimental U-O bond length in bulk UO_2.

Multiple water molecules adsorb in a broadly similar way to single molecules, as there is little interaction between them. However, for two water molecules adsorbing, one molecularly and one dissociatively, the H-O distance between the hydrogen of

the adsorbed water molecule and the oxygen of the adsorbed hydroxide species is 1.81 Å, suggesting a hydrogen bond between the two adsorbates.

Water adsorbs on the PuO_2 (111) surface in a similar way to the UO_2. For molecular adsorption the Pu-O_W distance is 2.50 Å, 0.07 Å shorter than the U-O_W distance, in agreement with the smaller ionic radius of Pu^{4+} *vs* U^{4+}, 0.96 Å and 1.00 Å respectively[42]. For dissociative adsorption the H-OH distance between the two hydroxyl species is 1.59 Å, and the Pu-O_{OH} distance is 2.20 Å, 0.01 Å shorter than the U-O_{OH} distance. This is slightly shorter than the length calculated by Rák *et al.* of 2.22 Å[15], however they also calculated the Pu-O_{OH} length to be shorter than the U-O_{OH} length, by 0.02 Å.

Adsorption Energies

Molecular and dissociative adsorption of energies of one water molecule were calculated on the $U_4U_{15}O_{38}$ cluster at the four sites shown in Figure 7, and are collected in Table 1. Note that the data for site 1 were reported in our previous paper[30]. The adsorption energy varies between the four sites, with two sites yielding energies 0.07-0.11 eV larger than the other two. As the energy differs depending on the adsorption site, for a given number of water molecules the same adsorption sites will be used when making comparisons between UO_2 and PuO_2.

	Adsorption Energy	
Site	Molecular	Dissociative
1	-1.04	-1.08
2	-1.11	-1.19
3	-1.12	-1.16
4	-1.05	-1.08

Table 1

Adsorption energies (eV) for a water molecule adsorbing either molecularly or dissociatively on the four different adsorption sites of the $U_4U_{15}O_{38}$ cluster (Figure 7).

The adsorption energies in Table 1 were calculated with the SV(P) basis set. We have previously tested the effect of basis set on the adsorption energy for molecular and dissociative adsorption, finding that increasing the basis set size up to the QZVP level significantly decreases the adsorption energy[30]. However, the size of the basis set had only a modest effect on the adsorption geometry, therefore we concluded that geometry optimizations could be performed at the SV(P) level, with single point energies calculated using larger basis sets. It should be noted that although the TURBOMOLE basis set library provides valence basis sets for the actinides from the SV(P) level up to QZVP, in fact the same basis, the QZVP, is used at each level. Hence the decreasing adsorption energies correspond to increasingly balanced basis sets.

In order to see if the significant adsorption energy differences arise as a function of basis set superposition error (BSSE) due to the imbalance between the relatively large basis set on the actinide ions and the smaller basis set on the oxygen and hydrogen atoms, we have calculated adsorption energies including the counterpoise correction (CP) at the SV(P) level. The counterpoise correction calculations are, computationally, significantly less expensive than the QZVP calculations.

Table 2 provides adsorption energies for 1 to 4 water molecules at the SV(P), QZVP and SV(P) + CP levels on the $U_{19}O_{38}$ cluster, at the geometries obtained at the

23

SV(P) level with the $U_4U_{15}O_{38}$ cluster. Also shown are energies at the SV(P) + CP including dispersion *via* the Grimme D3 parameters (SV(P) + CP + D3). No data are given for two waters adsorbing molecularly (2m) or for four waters adsorbing either molecularly (4m) or dissociatively (4d), as these configurations relaxed to those in which one adsorption is molecular and one dissociative (1m,1d), three are molecular one dissociative (3m,1d) and one is molecular three dissociative (1m,3d), respectively.

Site	Type	SV(P)	QZVP	SV(P) + CP	SV(P) + CP + D3
1	1m	-1.06	-0.58	-0.52	-0.70
	1d	-1.24	-0.84	-0.63	-0.81
1,2	2m	-	-	-	-
	1m,1d	-1.24	-0.77	-0.78	-0.97
	2d	-1.12	-0.65	-0.56	-0.74
1,2,3	3m	-1.10	-0.61	-0.64	-0.83
	2m,1d	-1.22	-0.69	-0.76	-0.95
	1m,2d	-1.17	-0.65	-0.68	-0.87
	3d	-1.07	-0.57	-0.53	-0.72
1,2,3,4	4m	-	-	-	-
	3m,1d	-1.19	-0.69	-0.71	-0.91
	2m,2d	-1.21	-0.70	-0.74	-0.94
	1m,3d	-1.15	-0.62	-0.68	-0.87
	4d	-	-	-	-

Table 2

Adsorption energies (eV) per molecule of water on a $U_{19}O_{38}$ cluster representation of the (111) surface of UO_2 within the PEECM. Type of adsorption is denoted by m for molecular or d for dissociative. The adsorption sites (see Figure 7) are given in the first column. Most stable adsorption configuration for each number of water molecules is highlighted in grey.

The energies calculated at the QZVP and the SV(P) + CP levels are in good agreement with each other, the difference between the two being less than 0.1 eV in all systems, except for the case of one water molecule adsorbing dissociatively where the energies differ by 0.21 eV.

As noted in the Introduction, a recent theoretical study probing adsorption on the UO$_2$ (111) surface calculated adsorption energies of -1.10 eV and -1.12 eV for molecular and dissociative adsorption respectively;[24] these energies agree well with the ones calculated here with the SV(P) basis set, differing by only 0.04 eV and 0.12 eV respectively. However when the larger QZVP basis set is used the energies differ by 0.52 eV and 0.28 eV respectively. The previous study used the LDA functional, which is known to overestimate binding energies, and is surely why larger adsorption energies were found. Another theoretical study, using the GGA+U approach, calculated adsorption energies of -0.60 eV and -0.68 eV for molecular and dissociatively adsorbed water,[25] much closer to the values obtained here with the QZVP basis set or with the SV(P) + CP. We calculated the mean absolute deviation of our values from those from Bo *et al.*[25] (for 1 water molecule or 4 molecules adsorbing); for SV(P) our values differ by 0.56 eV from theirs, whilst for QZVP and SV(P) + CP they differ by 0.08 eV and 0.10 eV respectively. Both SV(P) + CP and QZVP therefore give very similar results and show good agreement with the periodic GGA+U values of Bo et *al.* Note that while the use of the QZVP basis set or the SV(P) + CP decreases the adsorption energy relative to the SV(P) approach, there is no effect on the relative ordering of the adsorption energies.

With one water molecule, dissociative adsorption is more favourable than molecular. However, for two or more water molecules adsorbing a mixture of molecular and dissociative adsorption is favourable on UO$_2$. This is in agreement with the two recent theoretical studies mentioned above, which found dissociative adsorption to be more favourable at low coverage whilst a mixture of molecular and dissociative adsorption is most favourable at higher coverage.[24,25]

The inclusion of the D3 dispersion corrections increases the adsorption energies by 0.18–0.20 eV, without changing the ordering in any of the energies obtained. It should be noted that the two previous DFT+U studies[24,25] with which we compare our energies, did not include dispersion effects.

Given the similarity of the QZVP and SV(P) + CP data to one another (and to the PBE+U results of Bo et al.[25]), and the much smaller computational cost of the CP calculations, we have used this approach throughout the rest of the study. Table 3 presents data for water adsorbing on the (111) surface of PuO_2. For one water molecule, molecular adsorption is more favourable than dissociative by 0.08 eV, by contrast to UO_2, for which dissociative adsorption is more favourable. For more than one water molecule, the all molecular cases are always more favourable than the all dissociative. However, as with UO_2, for two or more adsorbing water molecules a mixture of molecular and dissociative adsorption is most favourable on PuO_2. It should be noted that the difference between the 1m and 1d adsorptions on PuO_2 (111) is smaller than some of the differences between QZVP and SV(P) + CP calculations for the UO_2 (111) surface; therefore we do not definitively predict molecular or dissociative adsorption, but stress that the difference between the types of adsorption is small, and that mixed adsorption tends to be most favourable.

Site	Type	SV(P) + CP	SV(P) + CP + D3
1	1m	-0.53	-0.77
	1d	-0.45	-0.68
1,2	2m	-0.52	-0.75
	1m,1d	-0.74	-0.99
	2d	-0.39	-0.63
1,2,3	3m	-0.53	-0.77
	2m,1d	-0.66	-0.90
	1m,2d	-0.62	-0.88
	3d	-0.42	-0.66
1,2,3,4	4m	-0.59	-0.83
	3m,1d	-0.55	-0.79
	2m,2d	-0.65	-0.90
	1m,3d	-0.55	-0.80
	4d	-0.32	-0.56

Table 3

Adsorption energies (eV) per molecule of water on the (111) surface of PuO_2 modelled as a $Pu_{19}O_{38}$ cluster for SV(P) + CP within the PEECM. Type of adsorption is denoted by m for molecular or d for dissociative. The adsorption sites (Figure 7) are given in the first column. The most stable adsorption configuration for each number of water molecules is highlighted in grey.

The inclusion of the D3 dispersion contributions causes an increase in the adsorption energy of 0.23–0.25 eV, a slightly larger effect than seen on the UO_2 surface. The larger effect of the D3 dispersion contributions on PuO_2 than UO_2 is likely due to the smaller lattice parameter of PuO_2, as well as the shorter distances between the water molecules and the PuO_2 surface.

Without D3, analogous adsorption energies are all larger on the UO_2 than PuO_2 surface, in agreement with previous theoretical studies which examined dissociative water adsorption on the (111) surface of AnO_2.[15,26] Some of the analogous adsorption energies are higher on PuO_2 than UO_2 when D3 is included (for 2 water molecules 1m,1d and for 3 water molecules 1m,2d), however generally the adsorption energies are still higher on UO_2.

The Mulliken charges of key atoms in the cluster have been calculated at the SV(P) level and are shown in Table 4, from which it can be seen that the partial charges differ by 0.02 a.u. or less between the two systems. These data suggest that the different adsorption energies are unlikely to be due to differences in ionic bonding.

As has been mentioned previously the ionic radius of 8 coordinate Pu(IV) is smaller than that of U(IV) by 0.04 Å, therefore we would expect the Pu-O bonds involving the actinide and adsorbed species should be shorter than the same U-O bonds. This is the case for molecular adsorption, with the $Pu-O_W$ bond 0.07 Å shorter than the U-O_W bond and we have similar adsorption energies between the two AnO_2 systems. However, for dissociative adsorption the $Pu-O_{OH}$ bond is only 0.01 Å shorter than the U-O_{OH} bond, this corresponds to a weaker dissociative adsorption energy on PuO_2 than UO_2.

Type of absorption	Atom	Mulliken charges/ a.u.	
		UO_2	PuO_2
1m	O_{water}	-0.62	-0.62
	H	0.45	0.46
	H	0.46	0.46
	An	1.39	1.38
1d	$O_{ads\ OH}$	-0.66	-0.64
	$H_{ads\ OH}$	0.39	0.40
	$O_{surf\ OH}$	-0.75	-0.74
	$H_{surf\ OH}$	0.48	0.48
	An	1.28	1.27

Table 4

Mulliken charges on key atoms in the $An_{19}O_{38}$ cluster representation of the AnO_2 (111) surface for adsorption of a single water molecule either molecularly or dissociatively. Type of adsorption is denoted by m for molecular or d for dissociative.

Water adsorption on the (110) surface of AnO$_2$ (An = U, Pu)

Geometries

The adsorption of one to four water molecules was investigated on an An$_4$An$_{21}$O$_{50}$ cluster representation of the (110) surface (Figure 9) to obtain adsorption geometries, and an An$_{25}$O$_{50}$ analogue cluster for adsorption energies, with different ratios of molecular and dissociative adsorption. We consider water adsorption at 4 actinide sites, where the actinide is coordinated by only the inner cluster region. As with the (111) surface, these 4 actinide atoms all have their 5f electrons treated explicitly, whilst the rest of the actinide atoms use 5f-in-core PPs.
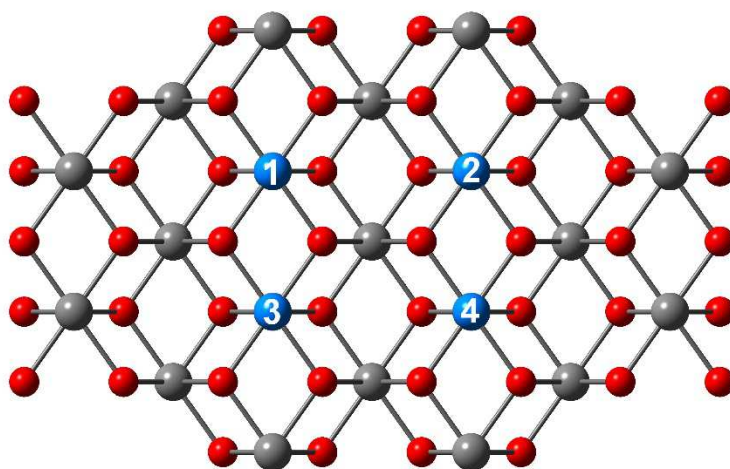

Figure 9

An$_4$An$_{21}$O$_{50}$ cluster viewed perpendicular to the (110) surface. Oxygen atoms are shown in red and actinide atoms in blue and grey. Grey spheres represent actinide atoms treated with 5f-in-core PPs. Embedding ions not shown. Sites where adsorption is considered are labelled 1 to 4.

The An$_4$An$_{21}$O$_{50}$ cluster has three layers of both actinide and oxygen atoms (Figure 10). The first layer contains 12 actinide atoms, eight of which are allowed to relax

during geometry optimizations, and 24 oxygen atoms, 14 of which are allowed to relax during geometry optimizations. The second layer has nine actinide atoms, one of which is allowed to relax during geometry optimizations, and 24 oxygen atoms, eight of which are allowed to relax. The third layer has four actinide atoms and two oxygen atoms, which are all fixed during geometry optimizations.

There are two types of adsorption on the (110) surface, as on the (111), molecular and dissociative. Molecular adsorption occurs with the hydrogen atoms tilted towards the surface, the oxygen atom is no longer directly above the actinide ion (Figure 10) but lies in the position of one of the two empty oxygen sites at each surface actinide atom. This increases the coordination of the surface actinide from 6 to 7. Dissociative adsorption again forms two hydroxides, the adsorbed hydroxide has its oxygen above the actinide ion and its hydrogen tilted towards a surface oxygen, whilst the surface hydroxide has its hydrogen angled towards another surface oxygen ion (Figure 10).
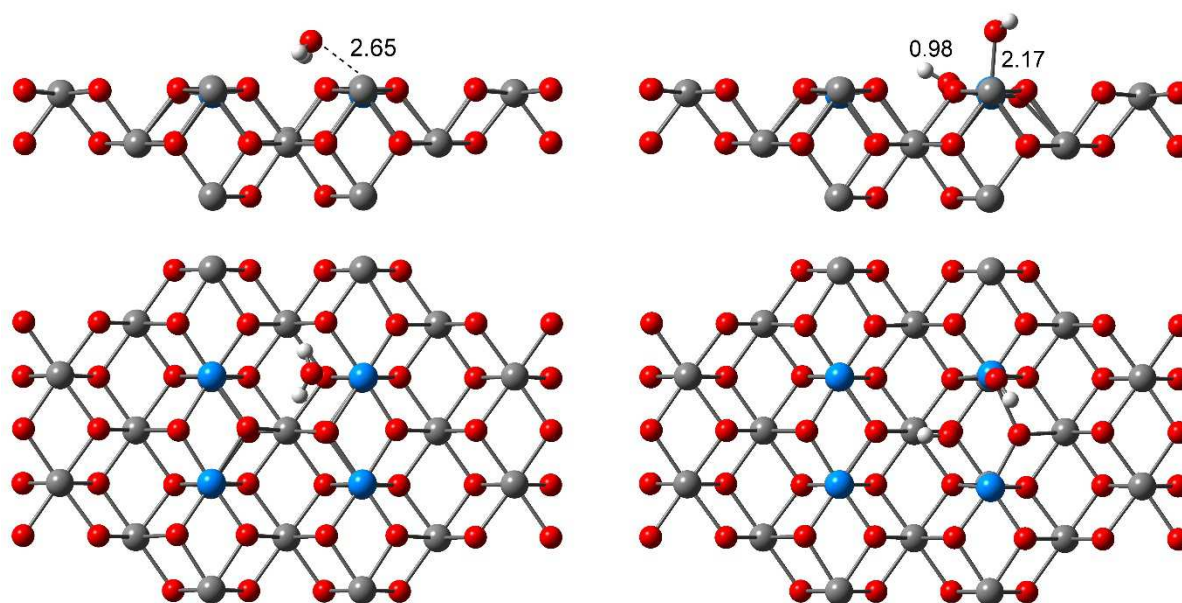
Figure 10

Molecular (left) and dissociative (right) adsorption of a single water molecule on the (110) surface of a $U_4U_{21}O_{50}$ cluster. Top view shows the cluster in the plane of the surface, whilst the bottom view is perpendicular to the surface. Hydrogen atoms are shown in white, oxygen atoms in red and actinide atoms in blue and grey. Grey spheres represent actinide ions treated with 5f-in-core PPs.

For the adsorption of one water molecule on UO_2 (110), the $U-O_W$ distance for molecular adsorption is 2.65 Å, 0.09 Å longer than on the (111) surface, whilst the $H-O_S$ distances are 1.78 Å and 2.13 Å forming a shorter and longer hydrogen bond between the adsorbed water and the surface oxygens. Bo *et al.* found a water molecule adsorbing almost perpendicular to the UO_2 (110) surface, with $U-O_W$ and $H-O_S$ distances of 2.64 Å and 1.61 Å respectively[25]; the $U-O_W$ value is only 0.01 Å different from that calculated here, however the $H-O_S$ distance here is 0.17 Å longer.

For the single dissociative adsorption the $U-O_{OH}$ distance is 2.17 Å, 0.04 Å shorter than on the (111) surface, whilst the $H-O_S$ is 0.98 Å. The bond distances calculated by Bo *et al.* for dissociative adsorption are in both cases identical to the ones calculated here.[25]

31

The Pu-O_W distance for one water molecule adsorbing molecularly on the (110) surface is 2.54 Å, 0.10 Å shorter than the U-O_W distance. The H-O_S length is also shorter on the PuO_2 surface at 1.73 Å. For dissociative adsorption the Pu-O_{OH} distance is 2.14 Å, 0.03 Å shorter than the U-O_{OH} distance, in agreement with the difference in ionic radii. Ràk *et al.* calculated a Pu-O_{OH} distance of 2.12 Å[15], in good agreement with our calculated value; their Pu-O_{OH} is 0.03 Å shorter than their U-O_{OH} distance, which we also find.

Adsorption Energies

Adsorption energies were calculated for different ratios of molecular and dissociative adsorption on the UO_2 (110) surface at the SV(P) + CP level on the $U_{25}O_{50}$ cluster, with the geometries obtained at the SV(P) level on the $U_4U_{21}O_{50}$ cluster, and are shown in Table 5, together with data including the D3 dispersion parameters.

Site	Type	SV(P) + CP	SV(P) + CP + D3
2	1m	-1.06	-1.29
	1d	-1.60	-1.77
1,4	2m	-0.96	-1.20
	1m,1d	-1.29	-1.47
	2d	-1.55	-1.70
1,2,4	3m	-0.97	-1.20
	2m,1d	-1.22	-1.41
	1m,2d	-1.16	-1.34
	3d	-1.54	-1.71
1,2,3,4	4m	-0.90	
	3m,1d	-1.02	-1.24
	2m,2d	-1.18	-1.39
	1m,3d	-1.27	-1.45
	4d	-1.34	-1.52

Table 5

Adsorption energies (eV) per molecule of water on the (110) surface of UO_2 modelled as a $U_{25}O_{50}$ cluster within the PEECM. Type of adsorption is denoted by m for molecular or d for dissociative. The adsorption sites (Figure 9) are given in the first column. Most stable adsorption configuration for each number of water molecules is highlighted in grey.

For one water molecule, dissociative adsorption is significantly more favourable than molecular. Bo *et al.* calculated a dissociative adsorption energy of -1.27 eV, 0.33 eV smaller than the value we calculate with SV(P) + CP. They also predict dissociative adsorption to be more favourable, calculating an energy for molecular adsorption of -0.62 eV, 0.44 eV smaller than our value.[25] This preference for dissociative adsorption also holds as we increase the number of water molecules; in each case dissociated water is most favourable.

Table 6 presents analogous data for PuO_2. On the (110) PuO_2 surface, as on the (110) UO_2, dissociative adsorption is more favourable than molecular adsorption; with four water molecules the difference is 0.23 eV between all molecular or all dissociative adsorption. A preference for dissociative adsorption was also concluded from experimental studies of water adsorption on PuO_2, and the dissociative adsorption energy was estimated to be -1.82 eV[21]. This is 0.60 eV larger than our SV(P) + CP data for four adsorbing water molecules, though the inclusion of dispersion corrections reduces the difference between experiment and theory to only 0.36 eV.

Site	Type	SV(P) + CP	SV(P) + CP + D3
2	1m	-0.94	-1.25
	1d	-1.34	-1.58
1,4	2m	-1.03	-1.37
	1m,1d	-1.13	-1.39
	2d	-1.28	-1.51
1,2,4	3m	-1.00	-1.32
	2m,1d	-1.12	-1.39
	1m,2d	-1.17	-1.41
	3d	-1.22	-1.45
1,2,3,4	4m	-0.99	-1.32
	3m,1d	-1.08	-1.37
	2m,2d	-1.16	-1.43
	1m,3d	-1.13	-1.37
	4d	-1.22	-1.46

Table 6

Adsorption energies (eV) per molecule of water on the (110) surface of PuO_2 modelled as a $Pu_{25}O_{50}$ cluster within the PEECM. Type of adsorption is denoted by m for molecular or d for dissociative. The adsorption sites (Figure 9) are given in the first column. Most stable adsorption configuration for each number of water molecules is highlighted in grey.

Previous theoretical studies have found the (110) surface to be less stable than the (111)[13–15], although it is more chemically active and higher water adsorption energies are obtained[15,25]. The present work agrees with this; adsorption energies are higher on the (110) than the (111) surface. On the (111) surfaces of both UO_2 and PuO_2 the dissociative and molecular adsorption energies are similar, however there is more of a distinction on the (110) surfaces, with a clear preference for dissociative over molecular adsorption.

Conclusions

In this contribution we have studied the bulk and surface properties of actinide dioxides using an embedded cluster approach that has not been previously applied to the 5f elements. This PEECM approach allows the straightforward inclusion of

hybrid DFT, in this case PBE0, which correctly reproduces the insulator properties of bulk UO_2, NpO_2 and PuO_2, giving good agreement with the experimental band gaps.

A model to study water adsorption on the low-index surfaces of UO_2 and PuO_2 ((111) and (110)) has been developed, and adsorption geometries and energies are found to be similar to those from recent DFT+U studies within the periodic boundary condition framework.

On the (111) surfaces we find that molecular and dissociative adsorption are similar in energy, with a mixture of the two being the most stable. On the (110) surface we see higher adsorption energies for both molecular and dissociative adsorption in comparison to the (111) surface, and a preference for dissociative adsorption in both actinide dioxide systems, in agreement with experimental suggestions that PuO_2 has a fully hydroxylated surface. The adsorption energy is generally seen to be slightly higher on the UO_2 surfaces than the PuO_2 surfaces. The inclusion of Grimme D3 dispersion parameters is seen to increase the adsorption energy in all cases without having an effect on the ordering of the energies.

Having obtained adsorption geometries and energies of water on low index actinide dioxide surfaces in good agreement with periodic DFT studies, we are now using our method to investigate multiple layers of water on the surfaces, as well as the adsorption of water at defects sites, such as oxygen vacancies. The embedded cluster method is particularly useful for the study of adsorption at such defect sites, as they can be studied free of periodic boundary condition restrictions. We look forward to reporting the results of these calculations in future papers.

Acknowledgements

References

[1] L. Cox, W. Ellis, R. Cowan, J. Allen, S. Oh, I. Lindau, et al., Valence-band photoemission in UO2 (111) near the 5d resonant photon energy, Phys. Rev. B. 35 (1987) 5761–5765. doi:10.1103/PhysRevB.35.5761.

[2] S.-W. Yu, J.G. Tobin, J.C. Crowhurst, S. Sharma, J.K. Dewhurst, P. Olalde-Velasco, et al., f-f origin of the insulating state in uranium dioxide: X-ray absorption experiments and first-principles calculations, Phys. Rev. B. 83 (2011) 165102. doi:10.1103/PhysRevB.83.165102.

[3] J.J. Joyce, T. Durakiewicz, K.S. Graham, E. Bauer, D.P. Moore, J.N. Mitchell, et al., 5f Electronic Structure and Fermiology of Pu Materials, MRS Proc. 1264 (2011) 1264–Z09–04. doi:10.1557/PROC-1264-Z09-04.

[4] J.C. Boettger, A.K. Ray, All-electron LCGTO calculations for uranium dioxide, Int. J. Quantum Chem. 80 (2000) 824–830. doi:10.1002/1097-461X(2000)80:4/5<824::AID-QUA30>3.0.CO;2-Z.

[5] K. Kudin, G. Scuseria, R. Martin, Hybrid Density-Functional Theory and the Insulating Gap of UO2, Phys. Rev. Lett. 89 (2002) 266402. doi:10.1103/PhysRevLett.89.266402.

[6] H. Nakamura, M. Machida, M. Kato, Effects of spin-orbit coupling and strong correlation on the paramagnetic insulating state in plutonium dioxides, Phys. Rev. B. 82 (2010) 155131. doi:10.1103/PhysRevB.82.155131.

[7] G. Jomard, B. Amadon, F. Bottin, M. Torrent, Structural, thermodynamic, and electronic properties of plutonium oxides from first principles, Phys. Rev. B. 78 (2008) 075125. doi:10.1103/PhysRevB.78.075125.

[8] B. Sun, P. Zhang, X.-G. Zhao, First-principles local density approximation + U and generalized gradient approximation + U study of plutonium oxides., J. Chem. Phys. 128 (2008) 084705. doi:10.1063/1.2833553.

[9] L. Petit, A. Svane, Z. Szotek, W.M. Temmerman, G.M. Stocks, Electronic structure and ionicity of actinide oxides from first principles, Phys. Rev. B. 81 (2010) 045108. doi:10.1103/PhysRevB.81.045108.

[10] Q. Yin, S. Savrasov, Origin of Low Thermal Conductivity in Nuclear Fuels, Phys. Rev. Lett. 100 (2008) 225504. doi:10.1103/PhysRevLett.100.225504.

[11] Q. Yin, A. Kutepov, K. Haule, G. Kotliar, S.Y. Savrasov, W.E. Pickett, Electronic correlation and transport properties of nuclear fuel materials, Phys. Rev. B. 84 (2011) 195111. doi:10.1103/PhysRevB.84.195111.

[12] I. Prodan, G. Scuseria, R. Martin, Covalency in the actinide dioxides: Systematic study of the electronic properties using screened hybrid density functional theory, Phys. Rev. B. 76 (2007) 033101. doi:10.1103/PhysRevB.76.033101.

[13] M. Abramowski, S. Redfern, R. Grimes, S. Owens, Modification of UO2 crystal morphologies through hydroxylation, Surf. Sci. 490 (2001) 415–420. doi:10.1016/S0039-6028(01)01368-1.

[14] A. Tan, R. Grimes, S. Owens, Structures of UO2 and PuO2 surfaces with hydroxide coverage, J. Nucl. Mater. 344 (2005) 13–16. doi:10.1016/j.jnucmat.2005.04.008.

[15] Z. Rák, R.C. Ewing, U. Becker, Hydroxylation-induced surface stability of AnO2 (An=U, Np, Pu) from first-principles, Surf. Sci. 608 (2013) 180–187. doi:10.1016/j.susc.2012.10.002.

[16] S.D. Senanayake, H. Idriss, Water reactions over stoichiometric and reduced UO2 (111) single crystal surfaces, Surf. Sci. 563 (2004) 135–144. doi:10.1016/j.susc.2004.06.169.

[17] S.D. Senanayake, G.I.N. Waterhouse, A.S.Y. Chan, T.E. Madey, D.R. Mullins, H. Idriss, The reactions of water vapour on the surfaces of stoichiometric and reduced uranium dioxide: A high resolution XPS study, Catal. Today. 120 (2007) 151–157. doi:10.1016/j.cattod.2006.07.040.

[18] S.D. Senanayake, R. Rousseau, D. Colegrave, H. Idriss, The reaction of water on polycrystalline UO2: Pathways to surface and bulk oxidation, J. Nucl. Mater. 342 (2005) 179–187. doi:10.1016/j.jnucmat.2005.04.060.

[19] J.M. Haschke, T.E. Ricketts, Adsorption of water on plutonium dioxide, J. Alloys Compd. 252 (1997) 148–156. doi:10.1016/S0925-8388(96)02627-8.

[20] J.L. Stakebake, Thermal desorption study of the surface interactions between water and plutonium dioxide, J. Phys. Chem. 77 (1973) 581–586. doi:10.1021/j100624a003.

[21] M. Paffett, D. Kelly, S. Joyce, J. Morris, K. Veirs, A critical examination of the thermodynamics of water adsorption on actinide oxide surfaces, J. Nucl. Mater. 322 (2003) 45–56. doi:10.1016/S0022-3115(03)00315-5.

[22] F.N. Skomurski, L.C. Shuller, R.C. Ewing, U. Becker, Corrosion of UO2 and ThO2: A quantum-mechanical investigation, J. Nucl. Mater. 375 (2008) 290–310. doi:10.1016/j.jnucmat.2007.12.007.

[23] P.F. Weck, E. Kim, C.F. Jové-Colón, D.C. Sassani, On the role of strong electron correlations in the surface properties and chemistry of uranium dioxide., Dalton Trans. 42 (2013) 4570–8. doi:10.1039/c3dt32536a.

[24] P. Maldonado, L.Z. Evins, P.M. Oppeneer, Ab Initio Atomistic Thermodynamics of Water Reacting with Uranium Dioxide Surfaces, J. Phys. Chem. C. 118 (2014) 8491–8500.

[25] T. Bo, J.-H. Lan, Y.-L. Zhao, Y. Zhang, C.-H. He, Z.-F. Chai, et al., First-principles study of water adsorption and dissociation on the UO2 (111), (110) and (100) surfaces, J. Nucl. Mater. 454 (2014) 446–454. doi:10.1016/j.jnucmat.2014.09.001.

[26] J.C. Boettger, A.K. Ray, Fully relativistic density functional calculations on hydroxylated actinide oxide surfaces, Int. J. Quantum Chem. 90 (2002) 1470–1477. doi:10.1002/qua.10350.

[27] G. Jomard, F. Bottin, G. Geneste, Water adsorption and dissociation on the PuO2 (110) surface, J. Nucl. Mater. 451 (2014) 28–34. doi:10.1016/j.jnucmat.2014.03.012.

[28] X. Wu, A. Ray, Density-functional study of water adsorption on the PuO2 (110) surface, Phys. Rev. B. 65 (2002) 085403. doi:10.1103/PhysRevB.65.085403.

[29] A.M. Burow, M. Sierka, J. Döbler, J. Sauer, Point defects in CaF2 and CeO2 investigated by the periodic electrostatic embedded cluster method, J. Chem. Phys. 130 (2009) 174710. doi:10.1063/1.3123527.

[30] J.P.W. Wellington, A. Kerridge, N. Kaltsoyannis, Embedded Cluster Calculations of Water Adsorption on the UO2 (111) Surface, in: WM2016 Proc., 2016.

[31] R. Ahlrichs, M. Bär, M. Häser, H. Horn, C. Kölmel, Electronic structure calculations on workstation computers: The program system Turbomole, Chem. Phys. Lett. 162 (1989) 165–169. doi:10.1016/0009-2614(89)85118-8.

[32] J.P. Perdew, K. Burke, M. Ernzerhof, Generalized Gradient Approximation Made Simple [Phys. Rev. Lett. 77, 3865 (1996)], Phys. Rev. Lett. 78 (1997) 1396–1396. doi:10.1103/PhysRevLett.78.1396.

[33] J.P. Perdew, M. Ernzerhof, K. Burke, Rationale for mixing exact exchange with density functional approximations, J. Chem. Phys. 105 (1996) 9982–9985. doi:10.1063/1.472933.

[34] A. Schäfer, H. Horn, R. Ahlrichs, Fully optimized contracted Gaussian basis sets for atoms Li to Kr, J. Chem. Phys. 97 (1992) 2571. doi:10.1063/1.463096.

[35] K. Eichkorn, F. Weigend, O. Treutler, R. Ahlrichs, Auxiliary basis sets for main row atoms and transition metals and their use to approximate Coulomb potentials, Theor. Chem. Acc. 97 (1997) 119–124. doi:10.1007/s002140050244.

[36] A. Moritz, X. Cao, M. Dolg, Quasirelativistic energy-consistent 5f-in-core pseudopotentials for divalent and tetravalent actinide elements, Theor. Chem. Acc. 118 (2007) 845–854. doi:10.1007/s00214-007-0330-6.

[37] F. Weigend, F. Furche, R. Ahlrichs, Gaussian basis sets of quadruple zeta valence quality for atoms H–Kr, J. Chem. Phys. 119 (2003) 12753. doi:10.1063/1.1627293.

[38] W. Küchle, M. Dolg, H. Stoll, H. Preuss, Energy-adjusted pseudopotentials for the actinides. Parameter sets and test calculations for thorium and thorium monoxide, J. Chem. Phys. 100 (1994) 7535–7542. doi:10.1063/1.466847.

[39] X. Cao, M. Dolg, H. Stoll, Valence basis sets for relativistic energy-consistent small-core actinide pseudopotentials, J. Chem. Phys. 118 (2003) 487. doi:10.1063/1.1521431.

[40] S. Grimme, J. Antony, S. Ehrlich, H. Krieg, A consistent and accurate ab initio parametrization of density functional dispersion correction (DFT-D) for the 94 elements H-Pu., J. Chem. Phys. 132 (2010) 154104. doi:10.1063/1.3382344.

[41] R.B. Ross, S. Gayen, W.C. Ermler, Ab initio relativistic effective potentials with spin–orbit operators. V. Ce through Lu, J. Chem. Phys. 100 (1994) 8145. doi:10.1063/1.466809.

[42] R.D. Shannon, Revised effective ionic radii and systematic studies of interatomic distances in halides and chalcogenides, Acta Crystallogr. Sect. A. 32 (1976) 751–767. doi:10.1107/S0567739476001551.

[43] X.-D. Wen, R.L. Martin, T.M. Henderson, G.E. Scuseria, Density functional theory studies of the electronic structure of solid state actinide oxides., Chem. Rev. 113 (2013) 1063–96. doi:10.1021/cr300374y.

[44] Y. Yun, J. Rusz, M.T. Suzuki, P.M. Oppeneer, First-principles investigation of higher oxides of uranium and neptunium: U3O8 and Np2O5, Phys. Rev. B - Condens. Matter Mater. Phys. 83 (2011) 1–10.

doi:10.1103/PhysRevB.83.075109.

[45] B.-T. Wang, H. Shi, W. Li, P. Zhang, First-principles LDA+U and GGA+U study of neptunium dioxide, Phys. Rev. B. 81 (2010) 045119. doi:10.1103/PhysRevB.81.045119.

[46] I.D. Prodan, G.E. Scuseria, J.A. Sordo, K.N. Kudin, R.L. Martin, Lattice defects and magnetic ordering in plutonium oxides: A hybrid density-functional-theory study of strongly correlated materials, J. Chem. Phys. 123 (2005) 014703. doi:10.1063/1.1953427.

[47] I.D. Prodan, G.E. Scuseria, R.L. Martin, Assessment of metageneralized gradient approximation and screened Coulomb hybrid density functionals on bulk actinide oxides, Phys. Rev. B - Condens. Matter Mater. Phys. 73 (2006) 1–10. doi:10.1103/PhysRevB.73.045104.

[48] J. Schoenes, Optical properties and electronic structure of UO2, J. Appl. Phys. 49 (1978) 1463. doi:10.1063/1.324978.

[49] T.M. McCleskey, E. Bauer, Q. Jia, A.K. Burrell, B.L. Scott, S.D. Conradson, et al., Optical band gap of NpO2 and PuO2 from optical absorbance of epitaxial films, J. Appl. Phys. 113 (2013) 013515. doi:10.1063/1.4772595.